PARAMETER IDENTIFICATION OF FLYING WING WITH SIGNIFICANT DEFORMATION

Balázs Gáti*, Miklós Somos**
***Dept. of Aircraft and Ships, Budapest University of Technology and Economics,**
**** Dept. of Chassis and Lightweight Structures, Budapest University of Technology and Economics**

Keywords: *elastic wing , multibody model, Vortex Lattice Method, parameter identification, HALE UAV*

Abstract

The in-flight deformation is a characteristic challenge in the design of the HALE UAVs. This paper deals with identifying the parameters of a multibody model of a flying wing of high aspect ratio, where the pressure distribution over the wing is calculated using a built-in Vortex-Lattice method in every step of the simulation. The identification is based on drop tests of a scale model of a flat wing and image processing.

1 Introduction

On the video footage showing flights of High Altitude Long Endurance Unmanned Aerial Vehicles (HALE UAV), one can observe that the wings do not really behave as rigid or classic elastic bodies. If some disturbance deforms the wing, the structure shows large deformation, and it takes a long time before the elastic forces put the wing back into the original shape. The extrapolation of this behavior gave the idea to develop a multibody model that can simulate the motion and deformation of the near-flexible or even fully flexible flying wings.

A flexible flying wing is unserviceable without appropriate flight and deformation controller. Constructing the above-mentioned model is the first step to develop such a control that can provide "virtual stiffness" for the wing, and supersedes the heavy wingspar. Thus, we can get a flying object with significantly improved payload/take-off-weight ratio, which is a critical parameter of HALE UAV's because of the power available.

2 Multibody Model

Patil and Hodges [1] applied intrinsic equations for the dynamics of a general, non-uniform, twisted, curved, anisotropic beam to model a highly flexible flying wing. The method described in this paper was based on a different approach.

The wing was partitioned spanwise into smaller bodies that were connected using ball joints, springs and dampers. (Fig. 1.) The system of equations includes the equation of motion of each body, with the boundary constraints defined by the connections and additional equations. The [2] gives a detailed description of the equation system, its solution, the necessary program written in MATLAB and the investigations to verify the model.

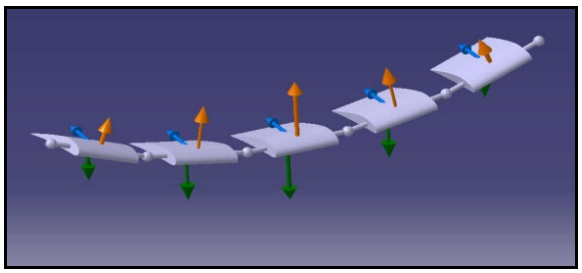

Fig. 1. Illustration of the multibody model

3 Aerodynamic Model

An adequate aerodynamic model has had to be choosen for the multibody simulation to obtain the forces which are taking effect on the wing.

3.1 Considerations, Selecting the Model

The selection of the applied model is based on three main conditions. First, the simulations are evaluated on a single PC platform, therefore the computational effort has to be kept as low as it can be. The flow around a three dimensional body submerged to the media is complex. Simplifications has to be taken which are conserving the important features of the flow. For example boundary layer, detached flows and vortex sheet roll-up are neglected. The second condition is that the model has to handle the complicated geometry generated by the multibody part of the simulation. It means that the calculations are performed on a twisted and bent surface. Finally the model should be easily improved including the above neglected effects. All these thoughts are induced the choice of a Vortex Lattice Method (VLM), precisely a steady VLM.

3.2 Theoretical Background

The VLM is based on the assumption that the flow around a body consists two main region at high Reynolds-numbers, the boundary layer in the immediate vincinity of the bounding surface, and the outer flow. It can be shown by the analysis of the Navier-Stokes equation, that the effects of viscosity are confined to a thin boundary layer and a thin wake after the body. Navier-Stokes equation with density (ρ) and viscosity (ν) independent from time and space coordinates:

$$\rho\frac{\partial \mathbf{c}}{\partial t}+\nabla^T\left(\mathbf{c}\circ\mathbf{c}^T\right)=\mathbf{f}-\nabla p+\nu\Delta\mathbf{c} \qquad (1)$$

By the transformation to a dimensionless form of the above expression, the Reynolds number appears in the last term:

$$\frac{1}{\mathrm{Re}}\Delta\mathbf{c} \qquad (2)$$

Detailing (2):

$$\frac{1}{\mathrm{Re}}\begin{pmatrix}\frac{\partial^2 u^*}{\partial x^{*2}}+\frac{\partial^2 u^*}{\partial y^{*2}}+\frac{\partial^2 u^*}{\partial z^{*2}}\\ \frac{\partial^2 v^*}{\partial x^{*2}}+\frac{\partial^2 v^*}{\partial y^{*2}}+\frac{\partial^2 v^*}{\partial z^{*2}}\\ \frac{\partial^2 w^*}{\partial x^{*2}}+\frac{\partial^2 w^*}{\partial y^{*2}}+\frac{\partial^2 w^*}{\partial z^{*2}}\end{pmatrix} \qquad (3)$$

(2) and (3) is often called diffusion. Viscosity causes the rotation of fluid. It is generated on the surface of the body, through the no slip condition. At high Reynolds number the viscous or diffusion term can be neglected, so rotation or vorticity is limited to a thin area as mentioned above.

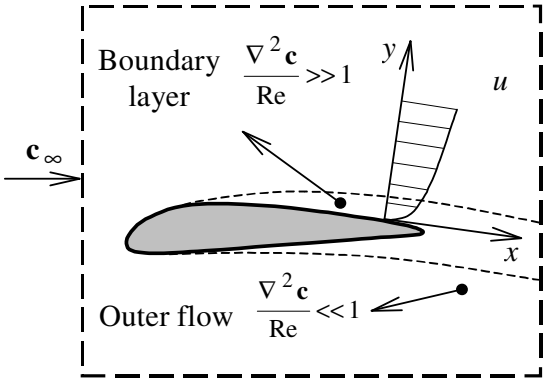

Fig. 2. Regions of flow

Therefore outer flow can be treated as being inviscid and irrotational, and its behaviour is described by:

$$\nabla^T\mathbf{c}=0 \qquad (4)$$

$$\frac{\partial \mathbf{c}}{\partial t}+\nabla^T\left(\mathbf{c}\circ\mathbf{c}^T\right)=\mathbf{f}-\frac{\nabla p}{\rho} \qquad (5)$$

Where (4) is mass conservation and (5) is momentum conservation equation.

3.3 General Solution, Discretization

The velocity field of an irrotational flow can be characterized by a velocity potential. There are two possible ways to formulate the problem:

$$\mathbf{c} = \nabla \times \mathbf{\Phi} \tag{7}$$

$$\mathbf{c} = \nabla \Phi \tag{8}$$

With the use of these expressions, (4) will take the form:

$$\nabla^2 \Phi = 0 \tag{9}$$

which is called Laplace's equation. It has to be solved on a given domain visualized on Fig. 3.

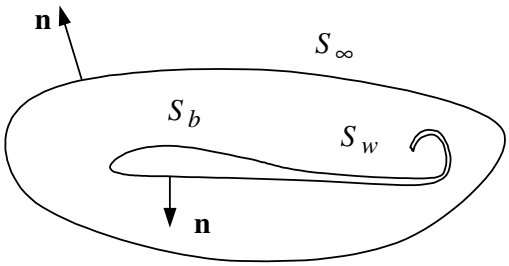

Fig. 3.

The solution requires to set up boundary conditions on S_b, S_w and S_∞:

$$\nabla \Phi \cdot \mathbf{n} = \mathbf{c}_b \cdot \mathbf{n} \tag{10}$$

$$\lim_{r \to \infty} \nabla \Phi = 0 \tag{11}$$

The flow through the surface of the body is zero (10), and the disturbance in the flow caused by the body decays to zero in the infinity (11). The general solution of Laplace's equation with the above boundary conditions can be gained by the application of Green's identity. Presuming that the body is thin:

$$\nabla \Phi(P) = \nabla \Phi_{b,w}(P) + \nabla \Phi_\infty(P) \tag{12}$$

$$\nabla \Phi_{b,w}(P) = \frac{1}{4\pi} \int_{S_b + S_w} \mu \nabla \left[\frac{\partial}{\partial n} \left(\frac{1}{r} \right) \right] dS \tag{13}$$

This solution automatically fullfills (11), therefore only (10) has to be applied on (12):

$$\nabla \Phi_b \cdot \mathbf{n} = \left[\mathbf{c}_b - \nabla \Phi_w \right] \cdot \mathbf{n} \tag{14}$$

$$\nabla \Phi_b = \int_{S_b} \frac{\mu}{4\pi} \nabla \left[\frac{\partial}{\partial n} \left(\frac{1}{r} \right) \right] dS \tag{15}$$

$$\nabla \Phi_w = \int_{S_w} \frac{\mu}{4\pi} \nabla \left[\frac{\partial}{\partial n} \left(\frac{1}{r} \right) \right] dS \tag{16}$$

(14) is the governing equation of the VLM. It contains integral quantities, which have to be discretized for calculating them on complicated surfaces. It can be done by subdividing the surface to quadrilateral elements or panels without gaps and overlappings.

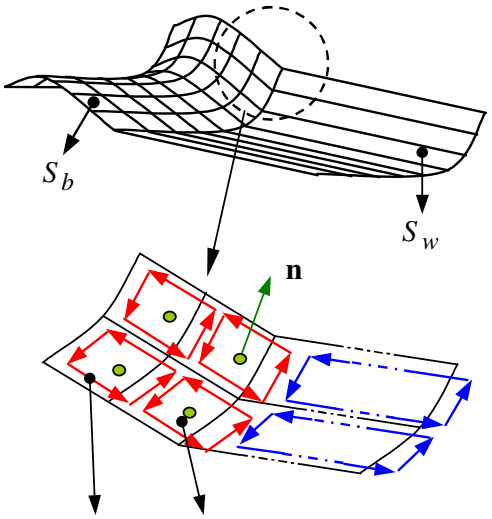

Fig. 4. Discretizing the geometry

Each quadrilateral on the surface of the body has a collocation point (P_i) and a normal vector ($\mathbf{n}_i$).

With the use of the panels defined above, equation (14), (15) and (16) yields:

$$\nabla\Phi_{b,i}\,\mathbf{n}_i = \left(\mathbf{c}_{b,i} - \nabla\Phi_{w,i}\right)\mathbf{n}_i \qquad (17)$$

$$\nabla\Phi_{b,i} = \sum_{j=1}^{N_b} \int_{panel} \frac{\mu_j}{4\pi} \nabla\left[\frac{\partial}{\partial n}\left(\frac{1}{r}\right)\right] dS \qquad (18)$$

$$\nabla\Phi_{w,i} = \sum_{k=1}^{N_w} \int_{panel} \frac{\mu_k}{4\pi} \nabla\left[\frac{\partial}{\partial n}\left(\frac{1}{r}\right)\right] dS \qquad (19)$$

In (18) and (19) the expression in the integrand is a constant strength (μ_j) doublet distribution. It can be proved that the latter element is equivalent to a vortex ring which is created by four straight vortex filaments placed on the edges of a doublet distribution (Fig. 4). The choice of the applied element is a matter of taste, maybe use of vortex lattice is more lifelike and forcibly descriptive.

Substituting (7) to (4) leads to:

$$\nabla\left(\nabla\times\Phi\right) = 0 \qquad (20)$$

A solution of (20) is the Biot-Savart law:

$$\mathbf{c} = \frac{\Gamma}{4\pi}\int_s \frac{d\mathbf{s}\times\mathbf{r}}{r^3} \qquad (21)$$

It gives the induced velocity of an arbritary vortex filament. For a finite length straight vortex filament (21) has to be applied in the form:

$$\mathbf{c} = \frac{\Gamma}{4\pi}\cdot\frac{\mathbf{r}_1\times\mathbf{r}_2}{\left|\mathbf{r}_1\times\mathbf{r}_2\right|^2}\cdot\left[\mathbf{r}\cdot\left(\frac{\mathbf{r}_1}{r_1}-\frac{\mathbf{r}_2}{r_2}\right)\right] \qquad (22)$$

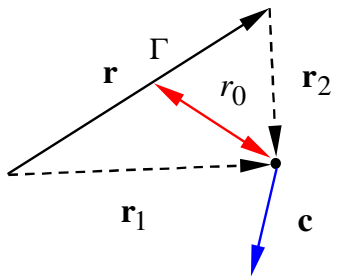

Fig. 5. Induced velocity of a vortex

3.4 System of Equations

If a vortex lattice is assembled of four straight vortex segment with Γ equal to unity and the induced velocity of it is signed by $\boldsymbol{C}$ then (17) become:

$$\sum_{j=1}^{N_b}\Gamma_{b\,j}\,\mathbf{C}_{b\,i,j}\cdot\mathbf{n}_i = \left[\mathbf{c}_{b\,i} - \sum_{k=1}^{N_w}\Gamma_{w\,k}\,\mathbf{C}_{w\,i,k}\right]\cdot\mathbf{n}_i \qquad (23)$$

The equation (23) is applied to the i-th collocation point, so there are N_b equation, which form an inhomogeneous linear system of equations:

$$\mathbf{C}_m\,\boldsymbol{\Gamma}_b = \mathbf{RHS} \qquad (26)$$

Where $\boldsymbol{C_m}$ is an $N_b \times N_b$ matrix, $\boldsymbol{\Gamma_b}$ is the vector of unknown panel circulations on the body. Solution of (24) for $\boldsymbol{\Gamma_b}$ is well known. In the present simulation a built-in MATLAB Moore-Penrose pseudoinverse procedure is used. The aerodynamic forces which are arising on the body panels, can be calculated from $\boldsymbol{\Gamma_b}$ with use of the Euler equation.

3.5 Handling of Unsteady Effects

The present aerodynamic calculation is a steady state method. It means that in each timestep the shedded vortex sheet is assumed to be like on Fig. 4. It follows, that such phenomenon as starting vortex, which has a quite strong circulation does not appear automatically in the simulation. The measurments have showed that this inadequacy significantly influences the difference between simulation and experiments. Therefore an additional formulae has to be applied to represent the starting vortex.

Lesson is that for an appropriate simulation an unsteady VLM is a minimum requirement. Fortunately the steady VLM can be easily upgraded to an unsteady method.

4 Identification

4.1 Drop Tests

A test wing (Fig. 6.) was built to validate the model and demonstrate the operability of the identification method developed for this purpose. The specifications were the following:

Span: 1035mm
Chord: 253mm
Profile: 3 mm thick flat plate with flap
Flap chord: 20%
Flap deflection: -8 deg (fixed)
Material: 3 mm thick depron foam.
Weight: 105 g

Fig. 6. The test wing

The wing was dropped from a start rig, which enabled the setting of the initial AoA and provided for reproducibility of drops. A small camera was mounted in the plane of symmetry, directed at the two markers on the wingtip. A second camera was installed to record the flight path of the wing from an external viewing point.

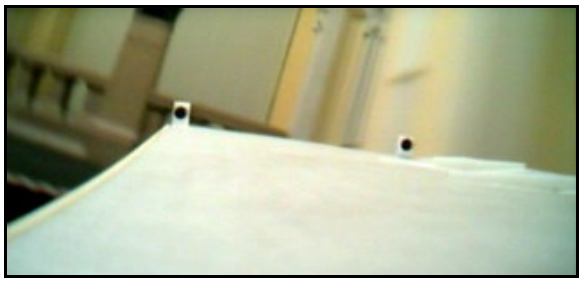

Fig. 7. Picture taken by the onboard camera

The footage of the two cameras were evaluated on two different ways. The recording of the onboard camera (Fig. 7.) were evaluated by a program based on the OpenCV computer vision library, written in the C language. This program was able to recognize the positions of the two black markers at the wingtip after applying specific filtering techniques. The camera and the method were calibrated by recognizing known wingtip deformations. The information on wingtip deformations enabled the identification of the elastic behavior of the wing material.

The footage from the ground camera were converted into sequence of images and the position of the wing was determined manually picture by picture. A long tape with equidistant markers was placed in different positions in the plane of flights to calibrate the camera. This way the distortion of the camera could also be eliminated. On the basis of the flight path, important parameters could be identified, which had effect on the moment coefficient of the wing.

Fig 8. shows the flight paths of ten different flights with the same initial conditions based on the evaluation of the recording of the ground based camera.

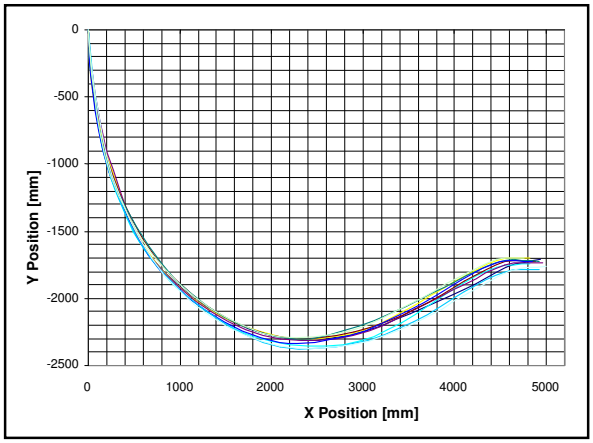

Fig. 8. Flight path of 10 drop tests

4.2 Simulation

Fig. 9. shows a simulated drop test with the initial values of the parameters in question (blue line) and the measured flight path (red crosses). The AoA by start was 11°.

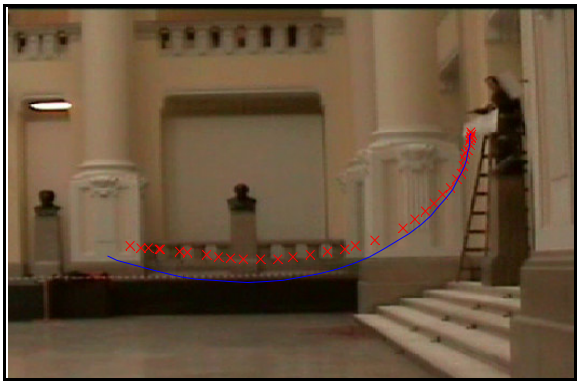

Fig. 9. Measured and first simulated flight path

The origin of the remarkable difference is the simplification in the Vortex Lattice Method used for calculating the pressure distribution over the wing. The airfoil used by the drop tests was a 3 mm thick flat plate profile with 20% chord flap. As opposed to the ideal flow modeled by the VLM, the viscous flow around the flat plate will separate at the leading edge of the wing, as was demonstrated in ANSYS CFX (Fig. 10.)

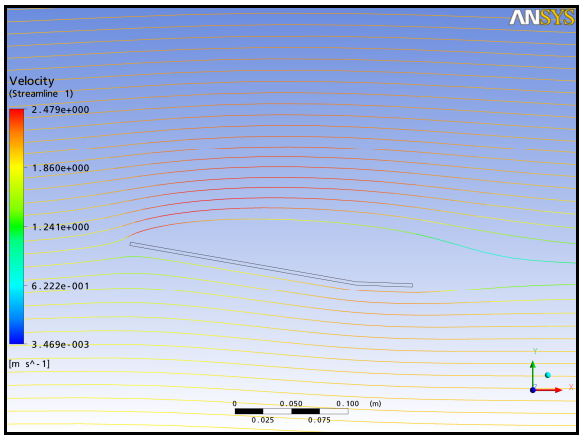

Fig. 10. Flow separation at the leading edge

The most important cause of the separation, is that the chordwise pressure distribution cannot properly be simulated using the VLM. To correct the error in the momentum equation caused by the false chordwise pressure distribution, a correction factor was applied to the flap deflection. This factor is the first target of our identification process.

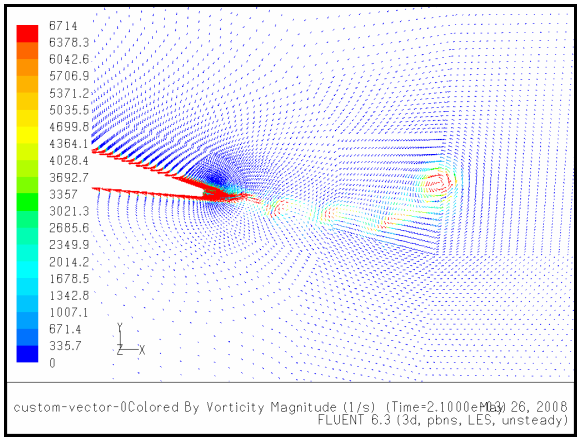

Fig. 11. Illustration of starting vortex [3]

The second aerodynamic effect that influenced the drop tests was the starting vortex (Fig. 11.). The starting vortex is the result of the rapid change in the circulation around the airfoil at the start. The induced velocity of an inviscid vortex is a function of $1/R$, where R is the radius. To take viscosity into account, we assumed a function of $1/R^2$. At the start, the velocity induced by the vortex significantly changed the flow along the chord and resulted in positive momentum. This momentum was modeled by an additional negative flap deflection, which was a function of k_2/R^2, where the value of k_2 was to be identified. The final flap deflection function applied was the following:

$$\delta_{Flsp} = \delta_0\left(1 + k_1 + \frac{k_2}{R^2}\right) \qquad (28)$$

The two parameters above influenced the flight path, therefore they could be identified from the recordings of the flight path. The onboard camera enabled the identification of additional parameters involved in the modeling of the flexible-elastic behavior of the wing. Our wing was made from depron, which is a kind of hard foam. Its Young modulus is hard to determine, thus it was difficult to calculate the spring coefficients of the virtual springs applied between the rigid bodies used for modeling the wing. As a result, the twisting and bending spring coefficients were the third and fourth parameters chosen for identification. The wing elasticity in the chordwise direction was significantly lower; therefore it was simply

approximated by a high spring coefficient, and was excluded from the target parameters of the identification process.

4.3 Identification Method

The identification method was based on the Nelder-Mead Simplex Method, and searched for the values of the chosen parameters at which the difference between the measured and simulated flight path and wingtip deformation is minimal. Two cost functions were applied:

$$C = \frac{\sum_{j=1}^{n}\left[\left(X_{S,i} - X_{M,i}\right)^2 + \left(Y_{S,i} - Y_{M,i}\right)^2\right]}{n} \quad (29)$$

$$C = \frac{\sum_{j=1}^{n}\left(Y_{wtS,j} - Y_{wtM,j}\right)}{m} \quad (30)$$

,where

X_S : simulated longitudinal positions of the CG in Earth based coordinate system (interpolated at the time of samples)

Y_S :simulated vertical positions of the CG in Earth based coordinate system (interpolated at the time of samples)

Y_{wtS} :simulated vertical deformations of wingtip (interpolated at the time of samples)

X_M :measured longitudinal positions of the CG in Earth based coordinate system

Y_M :measured vertical positions of the CG in Earth based coordinate system

Y_{wtM} :measured vertical deformations of wingtip

n,m :number of samples during the drop test

The (29) was applied to identify the parameters describing the effect of the starting vortex and the separated flow, while (30) was used to identify the two parameters describing the elastic behavior of the wing.

4.4 Results

Fig. 12. shows how the identification method searched for k_1 and k_2.

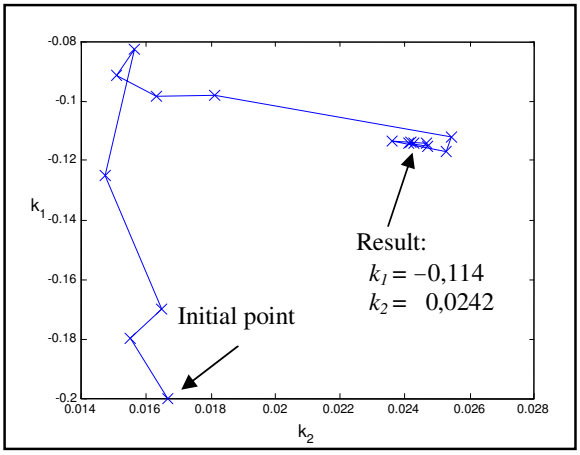

Fig. 12. Looking for k_1 and k_2

The resulted value of k_1 means that the effective flap deflection was reduced by 11,4 % because of the flow separation. The value of k_2 means that the effect of the starting vortex dropped after 0,49 m flight. Fig. 13. presents the simulated flight path with the resulted values of k_1 and k_2 (blue line) together with the measured one (red crosses).

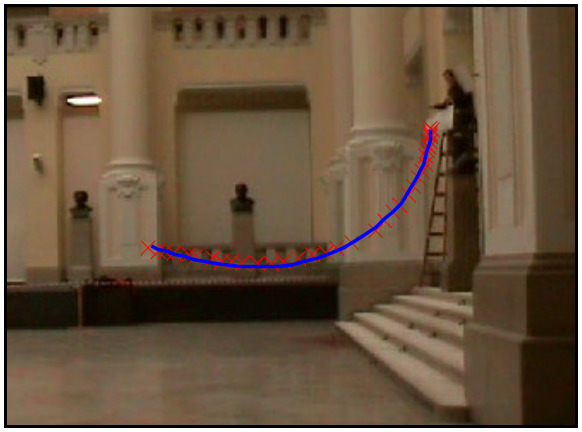

Fig. 13. Flight path after identification

Fig. 14. shows how the identification searched for the values of the spring coefficients, while Fig. 15. and Fig. 16. show the results.

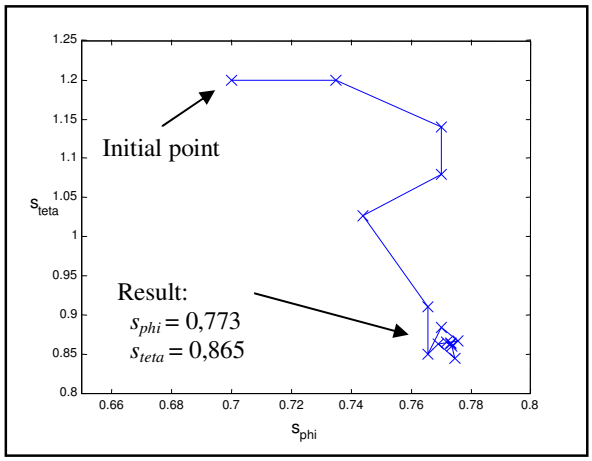

Fig. 14. Looking for the spring coefficients

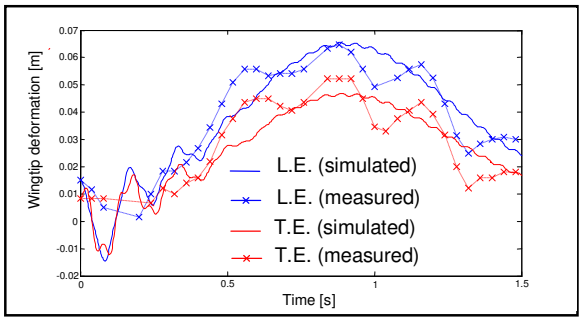

Fig. 15. Simulated and measured dihedral

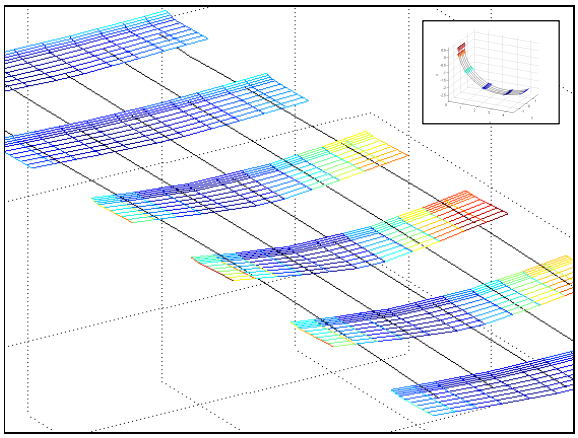

Fig. 16. Samples of the wing shape acquired in the simulated drop

5 Summary

The multibody model developed and the identification method was tested through drop tests of a scale model of a flying wing. The drops with different AoA were not evaluated in detail, but the results are promising enough to enable the entering the next phase of the development. This means that the unsteady VLM and the structural damping can be integrated into the simulation. On the practical side, the building of a large radio-controlled model can be started in order to test and demonstrate the flight and deformation controller under development.

References

[1] Patil, M. J., Hodges, D. H. "Flight Dynamics of Highly Flexible Flying Wings," In Proceedings of the International Forum on Aeroelasticity and Structural Dynamics, Munich, Germany, June 2005.

[2] Gáti, B., Multibody model of flying wing with significant deformation, *ICAS Conference*, Hamburg, , 2006.

[3] Personal communication with Regert, T.

Copyright Statement

The authors confirm that they, and/or their company or institution, hold copyright on all of the original material included in their paper. They also confirm they have obtained permission, from the copyright holder of any third party material included in their paper, to publish it as part of their paper. The authors grant full permission for the publication and distribution of their paper as part of the ICAS2008 proceedings or as individual off-prints from the proceedings.